LETTERS

Evidence for seismogenic fracture of silicic magma

Hugh Tuffen[1,2], Rosanna Smith[2] & Peter R. Sammonds[2]

It has long been assumed that seismogenic faulting is confined to cool, brittle rocks, with a temperature upper limit of ~600 °C (ref. 1). This thinking underpins our understanding of volcanic earthquakes, which are assumed to occur in cold rocks surrounding moving magma. However, the recent discovery of abundant brittle–ductile fault textures in silicic lavas[2–4] has led to the counter-intuitive hypothesis that seismic events may be triggered by fracture and faulting within the erupting magma itself. This hypothesis is supported by recent observations of growing lava domes, where microearthquake swarms have coincided with the emplacement of gouge-covered lava spines[5,6], leading to models of seismogenic stick-slip along shallow shear zones in the magma[7]. But can fracturing or faulting in high-temperature, eruptible magma really generate measurable seismic events? Here we deform high-temperature silica-rich magmas under simulated volcanic conditions in order to test the hypothesis that high-temperature magma fracture is seismogenic. The acoustic emissions recorded during experiments show that seismogenic rupture may occur in both crystal-rich and crystal-free silicic magmas at eruptive temperatures, extending the range of known conditions for seismogenic faulting.

Hundreds or thousands of small (magnitude $M < 3$), low-frequency earthquakes occur during lava dome growth, typically tightly clustered around the conduit and dome <2 km from the surface[8–11]. Events are commonly grouped in swarms, with similar waveforms indicating repeated activation of a near-static source[4,9,10]. The source mechanisms of these events have long been controversial, as strong attenuation in volcanic edifices makes full waveform inversions difficult and many potential mechanisms arise from the presence of interacting gas, liquid and solid phases[12].

Researchers have recently recognized that small-scale brittle–ductile faults are abundant in silica-rich lavas[3] and display remarkably similar characteristics to tectonic faults inferred to have been seismogenic. This raises the possibility that syn-eruptive seismicity is triggered by a process analogous to tectonic faulting[4]. This trigger mechanism unifies existing, competing models, as faults nucleated by magma fracture[2,13] would involve stick- or creep-slip deformation[7,14], while providing permeable pathways for transient escape of volcanic gases[2,3].

The faulting hypothesis is further supported by recent observations of dome growth at Mount St Helens and Unzen, where shallow seismic swarms coincided with lava spine extrusion along gouge-covered fault surfaces in the hot lava itself[5,6]. A growing number of researchers have thus proposed that fracturing of high-temperature, eruptible lava must control seismic triggering[2–4,13,15], while also controlling the dynamics of dome emplacement[7] and degassing patterns[16].

To test this hypothesis, we have done uniaxial and triaxial deformation experiments on samples of both glassy and crystalline lavas at temperatures up to 900 °C (Table 1). The glassy lava was aphyric bubble-free rhyolitic obsidian from Krafla, Iceland (100% glass), and the crystalline lava was porphyritic andesite (21% phenocrysts <2.5 mm long, <2% glass) from Mt Shasta, California. Further sample details are given in Supplementary Information.

Cylindrical samples 75 mm in length and 25 mm diameter, jacketed in a ductile iron sleeve, were deformed in compression in a high-pressure, high-temperature triaxial cell[17]. The sample dimensions greatly exceeded maximum crystal sizes, thus providing representative mechanical data. In triaxial tests, an all-round hydrostatic pressure was first applied to the sample and maintained at a set value (the 'confining pressure'), and then the sample was heated and maintained at a set temperature using an internal heater. An axial load was applied to the rock sample by a 200-kN servo-controlled pressure-balanced actuator at constant displacement rate (that is, constant strain rate). Acoustic emissions were detected continuously using a piezoelectric transducer attached to the loading piston via a waveguide. The use of a waveguide, which was essential to prevent high temperatures damaging the transducer, attenuates the acoustic signal but does not change the overall acoustic-emission frequency–magnitude relationships[18]. Samples were deformed at a range of constant strain rates (from $10^{-4.3}$ to 10^{-5} s^{-1}, with total strains of ≤4%) and temperatures in order to attain both brittle and ductile deformation behaviour (Table 1).

Figure 1 shows the results of deformation experiments done on obsidian at 645 °C, close to its glass transition. At the higher strain rate of $10^{-4.3}$ s^{-1} (Fig. 1a), initial quasi-elastic loading was followed by brittle–ductile behaviour characterized by a sequence of small, abrupt stress drops and associated reduction in compliance, which indicates progressive damage in the sample[19]. There is a clear correlation between stress drops and bursts of acoustic emission shown by the steps in the cumulative acoustic energy release (Fig. 1a), which we attribute to cracking in the sample. The seismic *b*-value (the log-linear slope of the acoustic-emission frequency–magnitude

Table 1 | Summary of experimental conditions

Sample	Material	Confining pressure (MPa)	Temperature (°C)	Strain rate (s^{-1})	Sample behaviour
SA45	Andesite	0.3	900	10^{-5}	Some ductile deformation, brittle shear failure
SA43	Andesite	10	900	10^{-5}	Predominantly ductile deformation with some shear cracking
SA42	Andesite	10	600	10^{-5}	Elastic–brittle
H15-3	Obsidian	0.3	645	$10^{-4.3}$	Some ductile deformation, axial cracking
H6	Obsidian	0.3	645	$10^{-4.9}$	Ductile barrelling
H15-4	Obsidian	0.1	20	10^{-5}	Elastic–brittle

[1]Department of Environmental Science, Lancaster University, Lancaster LA1 4YQ, UK. [2]Department of Earth Sciences, University College London, Gower Street, London WC1E 6BT, UK.

distribution, calculated here using Aki's maximum likelihood method[20]) decreases as the peak stress is approached. This decrease is indicative of microcrack extension and coalescence occurring with ongoing sample deformation[21]. A representative acoustic-emission waveform and power spectrum are shown in Fig. 1b. Energy is predominantly in the 100–300 kHz range. The onset is abrupt, and the waveform is typical of acoustic-emission events recorded during brittle failure of other crustal rock samples[22] and similar to waveforms we recorded during brittle failure of the obsidian at room temperature (Supplementary Information). Post-experiment sample analysis showed that numerous predominantly axial cracks had formed, with curved, conchoidal surfaces and local zones of cataclasis where slip had occurred between major subparallel cracks (Fig. 1c, upper image). Scanning electron microscopy (SEM) images of surfaces (Fig. 1c, lower image) show micrometre-scale hackle markings typical of brittle glass fracture[23]. At lower strain rates of $10^{-4.9}\,s^{-1}$ (Fig. 1d), ductile deformation of the sample occurred after initial quasi-elastic loading, leading to sample barrelling but without crack formation. No acoustic emissions were detected during such ductile behaviour. The sustained peak stress of 140 MPa at this strain rate reflects the melt viscosity of $\sim 10^{13}$ Pa s. Such strongly strain-rate-dependent ductile–brittle behaviour is typical of silicate melts[24].

Figure 2a shows the results of a deformation experiment on andesite at 900 °C. After a prolonged phase of quasi-elastic loading, the sample undergoes strain hardening (~0.37% strain) close to peak stress (of around 90 MPa) accompanied by strong acoustic-emission activity (Fig. 2a). Post-peak stress, the sample underwent a small but significant phase of 0.06% strain softening deformation and accelerating acoustic-emission activity, leading to dynamic failure. Failure involved the formation of a single shear fault at 17° to the loading axis. The *b*-value dropped to a local minimum at peak stress, recovered during strain softening deformation, before reaching a lower minimum as the sample failed. The *b*-value 'double minimum' is attributed to an increase in acoustic-emission amplitudes and crack tip stress intensities during pre-peak stress loading, which then

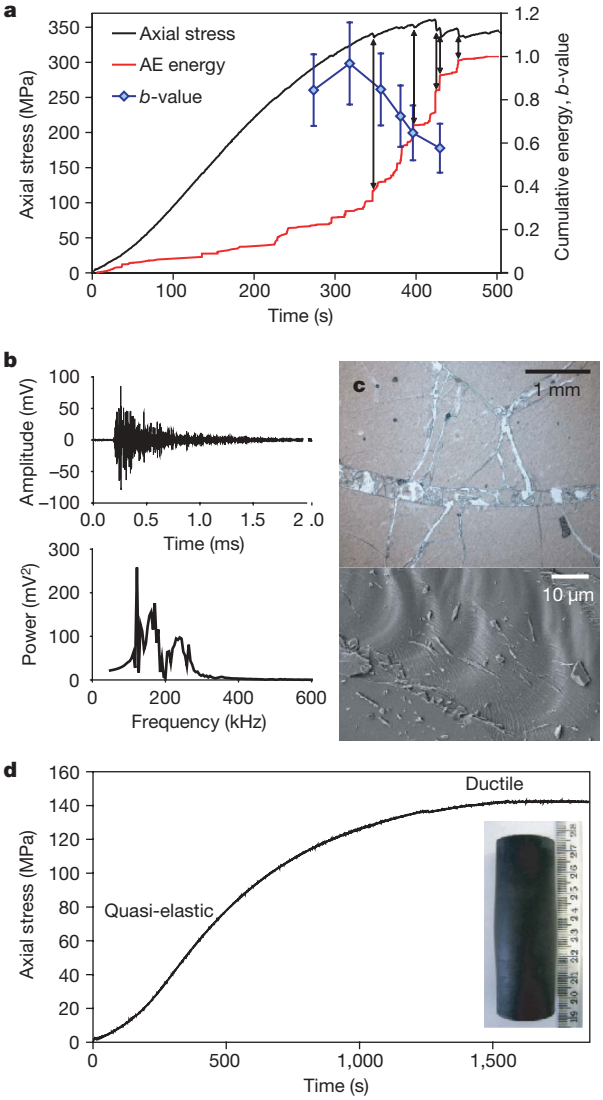

Figure 1 | Experimental results from high-temperature fracture of rhyolitic obsidian. **a**, Axial stress, normalized cumulative acoustic-emission (AE) energy, and acoustic-emission *b*-values against time for uniaxial deformation of rhyolitic obsidian at 645 °C and $10^{-4.3}\,s^{-1}$. Jumps in cumulative energy correspond with stress drops (arrows) and drops in compliance, indicating that cracking of the sample is associated with release of acoustic energy. Error bars show 95% confidence limits. **b**, Waveform (top) and power spectrum (bottom) of a typical acoustic-emission event, showing the sharp onset and high frequency content (predominantly 100–300 kHz) that are characteristic of brittle failure. **c**, Photomicrograph (top) of post-experiment obsidian sample H15-3, sectioned normal to applied load, showing formation of gouge on curved brittle fracture surfaces; SEM image (bottom) showing detail of typical fracture surface. **d**, Loading behaviour of obsidian deformed at 645 °C and $10^{-4.9}\,s^{-1}$, showing ductile deformation that led to barrelling of the sample H6 (inset; scale in cm).

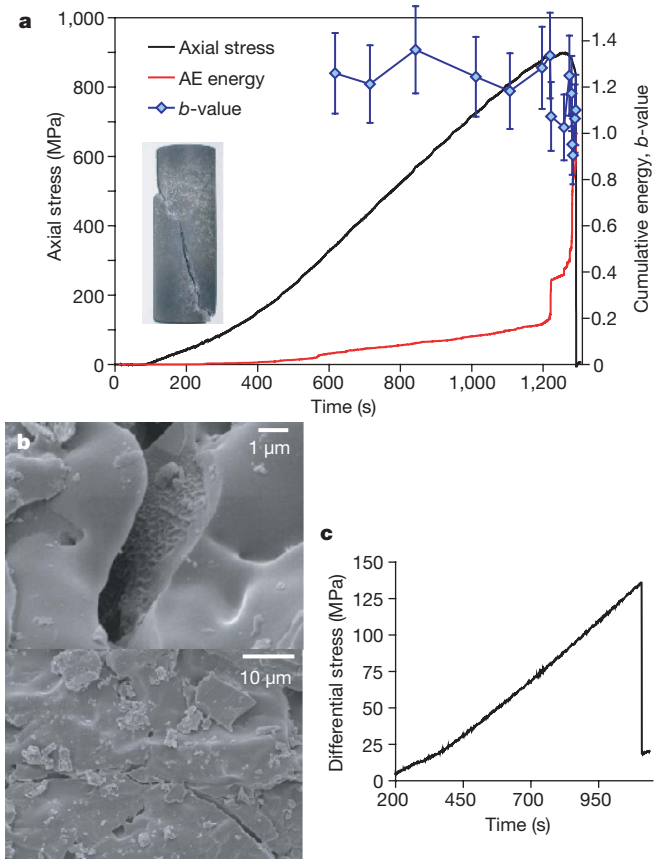

Figure 2 | Experimental results from high-temperature fracture of Mt Shasta andesite. **a**, Axial stress, normalized cumulative acoustic-emission energy, and acoustic-emission *b*-values against time for uniaxial deformation of Mt Shasta andesite (sample SA45) at 900 °C and $10^{-5}\,s^{-1}$. The sudden increase in acoustic-emission energy occurs close to peak stress, and the *b*-value drops sharply at failure. The post-experiment sample displays a through-going shear fracture (inset). Error bars show 95% confidence limits. **b**, SEM images of fracture surfaces in andesite deformed at 900 °C. Top, brittle–ductile textures preserved in glass on the shear fracture plane in SA43; bottom, quenched melt on a fracture surface in sample SH45. **c**, Differential stress against time for triaxial deformation of Mt Shasta andesite (sample SA42) at 600 °C and $10^{-5}\,s^{-1}$ with 10 MPa confining pressure. Brittle failure occurs immediately after the peak stress.

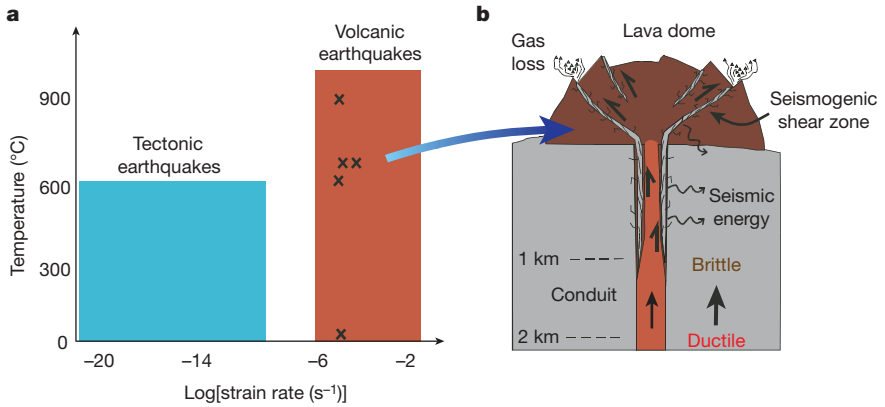

Figure 3 | Schematic diagrams comparing faulting in silicic magma to tectonic faulting and showing where fault zones may develop during a lava dome eruption. a, Diagram showing the approximate range of temperatures and strain rates for seismogenic faulting in the lithosphere as a whole ('tectonic earthquakes') and in silicic magma ('volcanic earthquakes'). Crosses indicate the conditions of the experiments described in this paper. **b**, Cartoon indicating how seismogenic fault zones develop in magma at the conduit walls and within lava domes, and act as pathways for gas escape.

dropped during strain softening deformation before increasing again at dynamic failure[25]. Post-experiment analysis using the SEM shows that brittle–ductile deformation of a melt phase had occurred on the fracture surface (Fig. 2b). In contrast, andesite samples deformed at 600 °C only exhibited 0.07% post-yield strain and failed immediately after reaching their peak stress (Fig. 2c).

Our experimental results extend the range of known conditions for seismogenic rupture to include magma at 900 °C (Fig. 3a). This is significantly greater than the 600 °C limit proposed for faulting elsewhere in the lithosphere[1], owing to compositional effects (the high viscosity of silicic magmas) and abnormally high strain rates in magma (about ten orders of magnitude faster than the lithosphere as a whole).

Recent conduit flow models[4,16] have shown that the high viscosity of silicic magma makes it prone to shear fracture during ascent in the shallow conduit, owing to the rheological stiffening of silicic magma driven by shallow degassing and crystallization[26]. This is consistent with the widespread field evidence for localized strain on shear zones in silicic magma, either at the conduit walls[2–4] or bounding lava spines[5,6]. Similar structures do not develop in more basic magma, owing to its lower viscosity[2].

Although volcano-tectonic earthquakes are generally thought to occur when cold rocks are fractured by moving magma[9], acoustic-emission waveforms recorded during our high-temperature experiments on obsidian have sharp onsets similar to volcano-tectonic earthquakes and their frequency content can also be scaled to volcano-tectonic events. Given that dominant frequencies of earthquakes scale inversely with source dimension[27], $d \times f$ (source dimension times frequency) should be the same for volcanic earthquakes and acoustic emission recorded in the laboratory if they have the same mechanism[28]. For a typical $M = 2$ volcano-tectonic earthquake, $d = 100$ m and $f = 15$ Hz, so $d \times f = 1.5 \times 10^3$ m Hz; for the experiments, $d = 0.01$ m and $f = 150$ kHz, so $d \times f = 1.5 \times 10^3$ m Hz, indicating the same brittle mechanism. The failure mode of experimental samples was predominantly tensile, whereas natural magmas often fail in shear[2–4,13,16]. However, the insight that the rupture is seismogenic is valid because shear failure typically generates more seismic energy than tensile failure for the same strain[29].

Shallow seismicity during lava dome eruptions is, however, dominated by low-frequency events (hybrid and long-period earthquakes, with dominant energy in the 1–10 Hz range). Source inversions[15] have shown that these events may constitute brittle failure events[2,13], and it has been speculated that the low frequencies reflect slow rupture of high-temperature magma[3,30]. Although we have not found any obvious difference in the frequency content of hot and cold failure events, further study is required to show whether rupture velocities show any temperature dependence. Alternatively, the low frequency content of hybrid and long-period earthquakes and their extended monochromatic codas may be attributed to conduit excitation[4,8,9] or path effects[15]. Magma fracture would, in this case, play a key role in creating transient permeable pathways for gas release and conduit excitation[2–4].

As demonstrated by the striking similarity between fault textures in magma and cooler crustal rocks[3,5], faulting in magma is analogous to seismogenic faulting elsewhere in the crust, despite occurring on dramatically shorter temporal and spatial scales (Fig. 3). Event magnitudes are limited by the dimensions of the magma body (hundreds of metres), and the lifetimes of individual faults are many orders of magnitude shorter than those of tectonic faults. Study of this hot, fast endmember of seismogenic faulting cycles may therefore shed light on faulting elsewhere in the lithosphere, as the evolution of short-lived swarms of similar events during dome eruptions[10] records the initiation and death of seismogenic fault systems.

Further experimentation is required to determine how seismic source characteristics and path effects (for example, rupture velocities and attenuation) relate to the mechanical state of the magma. This will greatly improve our understanding of how volcanic earthquakes relate to potentially hazardous changes in activity. It will also provide new insights into the mechanisms of a newly discovered type of seismogenic faulting.

Received 3 December 2007; accepted 2 April 2008.

1. McKenzie, D., Jackson, J. & Priestley, K. Thermal structure of oceanic and continental lithosphere. *Earth Planet. Sci. Lett.* **233,** 337–349 (2005).
2. Tuffen, H., Dingwell, D. B. & Pinkerton, H. Repeated fracture and healing of silicic magma generate flow banding and earthquakes? *Geology* **31,** 1089–1092 (2003).
3. Tuffen, H. & Dingwell, D. B. Fault textures in volcanic conduits: Evidence for seismic trigger mechanisms during silicic eruptions. *Bull. Volcanol.* **67,** 370–387 (2005).
4. Neuberg, J. *et al.* The trigger mechanism of low-frequency earthquakes on Montserrat. *J. Volcanol. Geotherm. Res.* **153,** 37–50 (2006).
5. Cashman, K. V., Thornber, C. R. & Pallister, J. S. in *A Volcano Rekindled: The First Year of Renewed Eruption at Mount St. Helens, 2004–2006* (eds Sherrod, D. R., Scott, W. E. & Stauffer, P. H.) Ch. 19 (USGS Professional Paper, US Geological Survey, Washington DC, in the press).
6. Nakada, S., Shimizu, H. & Ohta, K. Overview of the 1990–1995 eruption at Unzen volcano. *J. Volcanol. Geotherm. Res.* **89,** 1–22 (1999).
7. Iverson, R. M. *et al.* Dynamics of seismogenic volcanic extrusion at Mount St Helens in 2004–2005. *Nature* **444,** 439–443 (2006).
8. Chouet, B. Long-period volcano seismicity: Its source and use in eruption forecasting. *Nature* **380,** 309–316 (1996).
9. Neuberg, J. Characteristics and causes of seismicity in andesite volcanoes. *Phil. Trans. R. Soc. Lond.* **358,** 1533–1546 (2000).
10. Umakoshi, K. *et al.* Seismic activity associated with the growth of the lava dome at Unzen volcano (November 1993 - January 1994) — grouping of earthquakes on the basis of cross-correlations among their waveforms. *Bull. Volcanol. Soc. Jpn* **47,** 43–55 (2002).

11. Smith, R., Kilburn, C. R. J. & Sammonds, P. R. Rock fracture as a precursor to lava dome eruptions at Mount St Helens from June 1980 to October 1986. *Bull. Volcanol.* **69,** 681–693 (2007).
12. McNutt, S. R. Volcanic seismology. *Annu. Rev. Earth Planet. Sci.* **33,** 461–491 (2005).
13. Goto, A. A new model for volcanic earthquake at Unzen volcano: Melt rupture model. *Geophys. Res. Lett.* **26,** 2541–2544 (1999).
14. Voight, B. *et al.* Magma flow instability and cyclic activity at Soufriere Hills volcano, Montserrat, British West Indies. *Science* **283,** 1138–1142 (1999).
15. Harrington, R. M. & Brodsky, E. E. Volcanic hybrid earthquakes that are brittle failure events. *Geophys. Res. Lett.* **34,** L06308, doi:10.1029/2006GL028714 (2007).
16. Gonnermann, H. M. & Manga, M. Explosive volcanism may not be an inevitable consequence of magma fragmentation. *Nature* **426,** 432–435 (2003).
17. Rocchi, V., Sammonds, P. R. & Kilburn, C. R. J. Fracturing of Etnean and Vesuvian rocks at high temperatures and low pressures. *J. Volcanol. Geotherm. Res.* **132,** 137–157 (2004).
18. Meredith, P. G. & Atkinson, B. K. Stress corrosion and acoustic emission during tensile crack propagation in Whin Sill dolerite and other basic rocks. *Geophys. J. R. Astron. Soc.* **75,** 1–21 (1983).
19. Main, I. G. A damage mechanics model for power-law creep and earthquake aftershock and foreshock sequences. *Geophys. J. Int.* **142,** 151–161 (2000).
20. Aki, K. Maximum likelihood estimate of b in the formula log N=a-bM and its confidence limits. *Bull. Earthq. Res. Inst. Univ. Tokyo* **43,** 237–239 (1965).
21. Main, I. G., Sammonds, P. R. & Meredith, P. G. Application of a modified Griffith criterion to the evolution of fractal damage during compressional rock failure. *Geophys. J. Int.* **115,** 367–380 (1993).
22. Read, A. D., Ayling, M. R., Meredith, P. G. & Murrell, S. A. F. Microcracking during triaxial deformation of porous rocks monitored by changes in rock physical properties, II. Pore volumometry and acoustic emission measurements on water saturated rocks. *Tectonophysics* **245,** 223–235 (1995).
23. Hull, D. *Fractography* (Cambridge Univ. Press, Cambridge, UK, 1999).
24. Webb, S. L. & Dingwell, D. B. Non-Newtonian rheology of igneous melts at high stresses and strain rates: Experimental results for rhyolite, andesite, basalt and nephelinite. *J. Geophys. Res.* **95,** 15695–15701 (1990).
25. Sammonds, P. R., Meredith, P. G. & Main, I. G. Role of pore fluids in the generation of seismic precursors to shear fracture. *Nature* **359,** 228–230 (1992).
26. Sparks, R. S. J. *et al.* Control on the emplacement of the andesite lava dome of the Soufriere Hills volcano, Montserrat, by degassing-induced crystallization. *Terra Nova* **12,** 14–20 (2000).
27. Aki, K. & Richards, P. G. *Quantitative Seismology: Theory and Methods* (Freeman and Co., San Francisco, California, 1980).
28. Burlini, L. *et al.* Seismicity preceding volcanic eruptions: New experimental insights. *Geology* **35,** 183–186 (2007).
29. McGarr, A. Seismic moments and volume changes. *J. Geophys. Res.* **81,** 1487–1494 (1976).
30. Uchida, N. & Sakai, T. Analysis of peculiar volcanic earthquakes at Satsuma-Iojima volcano. *Earth Planets Space* **54,** 197–209 (2002).

Supplementary Information is linked to the online version of the paper at www.nature.com/nature.

Acknowledgements We are grateful to J. Bowles, S. Boon and N. Hughes for technical assistance with the experiments, C. Kilburn and H. Pinkerton for discussions and W. Hirt for help during fieldwork on Mt Shasta. This research was supported by the UK Natural Environment Research Council and the Leverhulme Trust (H.T.).

Author Contributions H.T. provided the initial idea, carried out deformation experiments on obsidian, analysed data and co-wrote the paper. R.S. carried out deformation experiments on andesite, analysed data and co-wrote the paper. P.R.S. co-wrote the paper and assisted with the experimental programme.

Author Information Reprints and permissions information is available at www.nature.com/reprints. Correspondence and requests for materials should be addressed to H.T. (h.tuffen@lancaster.ac.uk).